Supporting information for **"Nanoscale pillar arrays for separations"**

Teresa B. Kirchner[†], Rachel B. Strickhouser[†], Nahla A. Hatab[†], Jennifer J. Charlton[ψ,†], Ivan I. Kravchenko[‡], Nickolay V. Lavrik[‡], and Michael J. Sepaniak*[,†]

[†]Department of Chemistry, University of Tennessee, Knoxville, TN, 37996, USA.

[‡]Center for Nanophase Materials Sciences, Oak Ridge National Laboratory, Oak Ridge, TN, 37830, USA.

[ψ] Y-12 National Security Complex, Analytical Chemistry Organization, Oak Ridge, TN 37830, USA

Table of Contents

1. Experimental details
    a. Nano-layer Array Fabrication
    b. C18 Functionalization
    c. Table 1: Nano-layer Array Parameters Investigated
    d. Table 2: Solvent Properties
    e. Development Chamber and Evaporation Considerations
    f. Spot and Solvent Flow Imaging
    g. Evaluation of Plate Height
    h. Image of pillars at the array boundary
2. Additional introduction and discussion
    a. Introduction & Solvent Flow Modeling
    b. Stacking
    c. Focusing

1. Experimental Section

a. Nano-layer Array Fabrication

The deterministic pillar arrays (DPA) were fabricated using standard cleanroom protocol for electron beam lithography, on silicon wafers using a JEOL JBX-9300FS EBL system. The master CAD file was created using Layout Editor where the pillars were designed to form equilateral triangles as reported in our earlier work[1-5] and by Desmet et. al. [6-10] A 300 nm-thick layer of ZEP520A e-beam resist (ZEON Chemical L.P., Japan) was spun on a 4-in silicon wafer and baked at 180°C for 2 min to harden the resist. The resist was patterned at an acceleration voltage of 100 kV and exposed to a dose of (420-450 μC/cm^2). After exposure, the resist was developed in Xylene for 30 sec, rinsed in isopropyl alcohol for another 30 s and dried under a stream of high-purity nitrogen. Following development, the wafer was exposed to oxygen plasma for 10 sec (Oxford reactive ion etcher) to clean residual resist from the channels[11]. For the lift-off process, a 20 nm Cr layer was first deposited using an electron-beam dual gun evaporation chamber (Thermonics Laboratory, VE-240) equipped with a quartz crystal monitor to measure the thickness. The excess resist and Cr were removed by lift-off using an acetone bath followed by isopropyl alcohol rinse.

The Si anisotropic RIE was carried out in an Oxford PlasmaLab system (Oxford Instruments, UK) at 10 mTorr in a SF6:C4F8:Ar mixture defined by respective flow rates of 58, 25 and 5 sccm. The wafer with Si pillars was then thermally annealed at ~600 ◦C for 10 min in a mixture of hydrogen and argon at a pressure of 735 Torr in a cold wall furnace (Easy Tube 3000, First Nano, Ronkonkoma, NY). Atomic layer deposition of SiO2 was carried out using an Oxford FlexAl tool to coat the resulting Si nanopillars with a 5 nm thick conformal layer. The wafer then was, again, thermally annealed at ~600◦C for 10min in a mixture of hydrogen and argon (10:1) at a pressure of 735 Torr in a cold wall furnace. A thin layer of

PSO (~25 nm) was then deposited on the wafer surface using a low temperature plasma enhanced chemical vapor deposition (System 100 Plasma Deposition Tool, Oxford Instruments) method[2]. The pillar dimensions were evaluated using a scanning electron microscope (Carl Zeiss, Merlin).

The nanoscale stochastic pillar arrays (SPA) were fabricated by using a unique lithography-free approach to fabricating pillar arrays. A thin layer (typically ~ 10 nm) of platinum was deposited on the silicon surface using physical vapor deposition. The Pt layer was then rapidly heated to ~900ºC in a cold wall furnace (Easy Tube 3000, First Nano, Ronkonkoma, NY) using a 10:1 ratio of argon and helium (P=735 torr). The thermally processed Pt islands that are created acted as a hard mask and the silicon wafer was then etched using the same anisotropic reactive ion etching and thin film deposition described in the electron beam lithography fabrication above, with further details available in previous work[12, 13]. The dimensions of the 5 cases investigated (with and without PSO and both types of arrays) are summarized in Table 1. It is noted that the dimensions in the table do not approach the limits of the fabrication techniques used herein. Pillar diameters and gaps can be considerably less than 100nm but may not be as stable as those used.

b. C18 Functionalization

The C18 reverse stationary phase was added to the arrays using a method described in our previous work[1] and by Hennion et. al. [14] where the arrays were pretreated using a 50:50 mixture of HNO_3 and HSO_4 acids to increase the number of surface silanols available for the C18 bonding. A 10% solution of the octadecyltrichlorosilane (C18) was prepared in toluene and heated to 170 ºC for 2 hours. The array was then rinsed with toluene, tetrahydrofuran, a 90/10% ratio of distilled water and tetrahydrofuran, and finally distilled water. Each rinse was for 10 minutes and repeated twice before continuing to the next rinse stage.

c. Table 1: Nano-array parameters investigated

Table 1. NTLC – Dimensions (pillar heights 1-2 μm)

Type	Diameter (nm)	Pitch (nm)	PSO
DPA	400	550	No
DPA	400	700	No
DPA	450	550	Yes
DPA	450	700	Yes
SPA	230 (RSD 41%)	640 (RSD 17%)	Yes

d. Table 2: Solvent Properties

Solvent	Polarity Index	Surface Tension (γ) mN/m	Viscosity (η) mPa s @25C	γ/ η ratio	Molecular Weight	Vapor Pressure (torr)
Benzyl Alcohol	4.07	39.00 @20C	5.474	7.12	108.14	0.11 @25C
Acetonitrile	5.8	28.66 @ 25C	0.369	77.67	41.05	100 @27C
2-Propanol	3.9	20.93 @ 25C	2.038	10.27	60.10	40 @ 23.8C
Ethanol	5.2	21.97@25C	1.074	20.46	46.07	50@25C

e. Development chamber

The horizontal development chamber was designed to minimize volume in order to inhibit evaporation issues. Aluminum metal was machined such that there was a trough of solvent surrounding the nanothin-layer array in order to create a uniform vapor environment. The chamber was sealed using a polydimethylsiloxane gasket and allowed to come to equilibrium. A moveable support was used that allowed for contact with the mobile phase to be made or interrupted to control the development. The volume is < 2mL total and allows for real time analysis of analyte development (SI Figure 1).

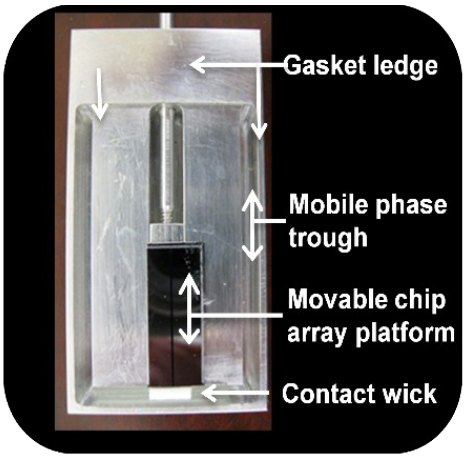

Figure 1: Horizontal development chamber.

Alternatively, vertical development can also be utilized by mounting the array to a moveable support and sealing inside of a more traditional vertical development chamber. After equilibrium is established the array is lowered to make direct contact with the mobile phase.

Further efforts to minimize evaporation issues within these chromatographic systems will be attempted through a variety of controlled experiments. These include changing the gasket thickness to precisely control the chamber volume and experimentation with temperature control of both the array and the chamber window to allow for the manipulation of solvent (vapor versus liquid) - array interactions in order to minimize evaporation problems. External partial or full saturation of solvent in an ambient gas, with flow in and out of the development chamber, will be pursued to maintain greater control of the local environment proximal to the pillar arrays.

f. Spot and solvent flow imaging

Fluorescence imaging of developed and developing spots for efficiency and separations evaluations was performed using a Nikon Eclipse E600 with Q capture software. Chromatograms were generated from these images using Image J 1.47V (Wayne Rashband, National Institutes of Health, USA) public domain software A . Solvent velocity was recorded using a Watec LCL-211H CCD camera coupled with GrabBee video capture software.

g. Evaluation of plate height

Plate heights for these nano-scale systems were evaluated using three different methods. The first two methods were similar to the analysis reported in our previous publication[1]. Both methods calculate H and peak capacity (n)[15] using the following equations:

$$H = \frac{(w_F - w_I)^2}{16d} \qquad [1]$$

$$n = 1 + \frac{(\sqrt{N})}{2} \qquad [2]$$

Where d is the distance the spot traveled and W_F and W_I are the final and initial spot widths (direction of flow), respectively. For the first method the plate height was evaluated by subtracting the initial spot

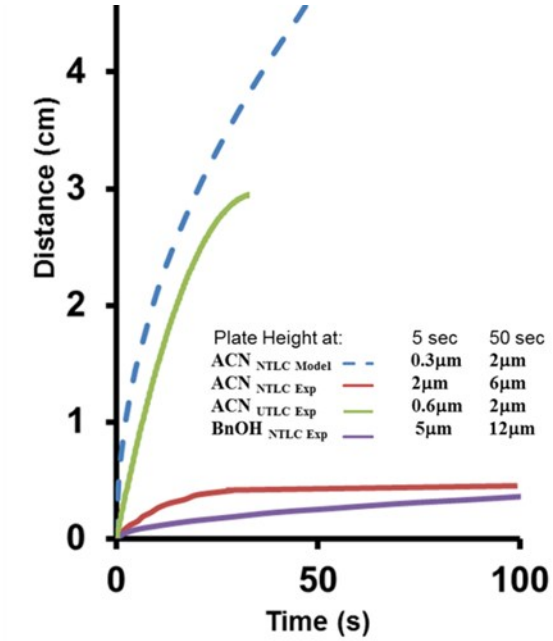

Figure 2: Flow rates and predicted plate heights.

width from the final width. The second method made the assumption that the initial spot width was infinitesimally small (W_I=0). This was due to the apparent improved efficiencies caused by focusing effects discussed below that caused the final band width to be narrower than the original spot width. The final method used the most prominent Van Deemter (B and Cm) terms that allowed predictions of efficiencies based on the solvent velocity data collected experimentally and modeled in the case of acetonitrile discussed more in Supporting Information. In all cases the calculated H represents a value averaged over the distance traveled. Equation 2 is is used often in chromatography as it relates peak capacity to plate number, N. Herein, N is determined via L/H and is used as a rough approximation of n despite the complication of a changing flow rate (hence efficiency) with position along the NTLC array.

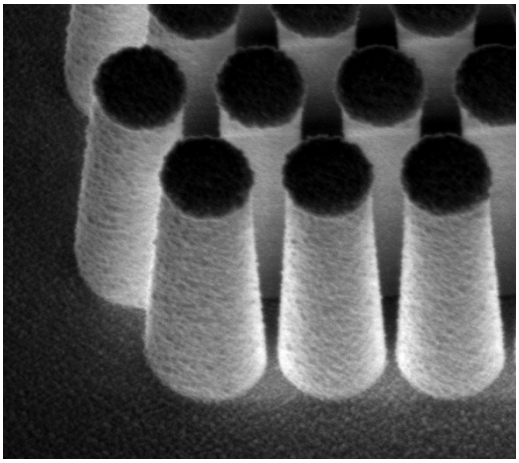

Figure 3: SEM of EBL sidewall.

h. Image of pillars at the array boundary.

After PSO deposition, SI Figure 3 demonstrates narrower gaps for the pillars that are on the boundary (pillars / no pillars). A few roows into the array the sidewalls of the pillars are nearly vertical. There is also PSO outside the array that can wick solvent. This heterogeneity can alter the flow rate in the boundary region of the array and produce irregular band fronts (see Figure 4A for example). Nevertheless, the central position of the bands remains uniform. This effect is not seen for the large DW arrays where the band does not encounter a boundary.

2. Additional introduction and discussion

a. Introduction & modeling

As discussed in our previous work the factors that contribute to plate height, H, are complex in planar chromatography [1, 16, 17]. The treatment that was used in order to validate the premise for this research was based on the well-known work proposed by Guiochon [18] and is often used as a thorough analysis for planar chromatography. This treatment is based on the validity of the Van Deemter equation (Equation [3]) that is common to HPLC theory.

$$H = A + \frac{B}{v} + (C_S + C_M)v \qquad [3]$$

From this equation H is dependent on eddy diffusion, A, longitudinal diffusion, B, which is influenced by the mobile phase velocity (v) and resistance to mass transfer in both the stationary and mobile phases, Cs and Cm, respectively. For the cases of highly ordered pillar arrays the eddy diffusion term (A) should be a minor factor that contributes to band broadening [1, 2]. For k'=0 or very thin stationary phases with rapid kinetics we can further exclude broadening contributions from the stationary phase term (C_S). As done in our previous publication we can use experimental literature values for the packing parameters of the pillar arrays of γ (0.5) and ω (0.02), [1, 2] the relevant plate height can be estimated based solely on the ubiquitous B and C_m terms by using Equation [4] with experimental or modeled knowledge of solvent velocity [1, 2, 19, 20].

$$H = \frac{2(\gamma)D_M}{v} + \frac{(\omega)d_p^2 v}{D_M} \qquad [4]$$

To further evaluate the predicted effect on efficiency and to further direct our chromatographic substrate development we derived wicking velocities by using the semi-empirical model developed by Mai et al. for ordered arrays of silicon pillars[21]. This model is based on the geometrical parameters of the fabricated substrate, experimentally measured solvent-substrate contact angles, and literature values for solvent

viscosity and surface tension. Modeled results were compared to the velocities that were experimentally observed in our system. In particular we calculated wicking velocities for acetonitrile and determined that the predicted solvent flow should result in improved plate heights; especially early in the solvent development.

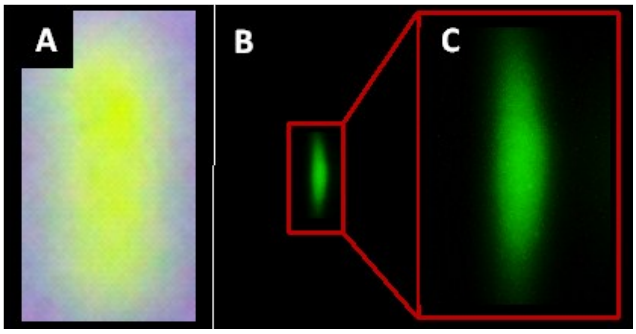

Figure 4: Illustration of stacking phenomena for NBD-heptyl amine; (**A**) reversed phase TLC case (spot width in flow direction ~2,300 µm), (**B**) stochastic array case (spot width ~400 µm), (**C**) B magnified ~ 4X.

We have estimated the plate heights for these nano-scale arrays using a typical diffusion coefficient (D_M) of 5.0E-6 cm^2/s for the solute, experimental velocities and modeled velocity for acetonitrile. The NTLC system plate heights are predicted to be smaller than the UTLC micro scale systems reported in our previous work[1] when using the same parameters for the packing factors and only changing the critical particle size (d_p) value (note: we use the inner pillar gap dimension) and using the modeled velocities for acetonitrile (SI Figure 2). These predicted plate heights are 0.3µm (NTLC) and 0.6 µm (UTLC) at 5 seconds and 1.7µm for both systems at 50 seconds. While the modeled case does not consider the porous SiO_2 layer and thus only roughly mimics the experiment, this treatment does indicated that the scaling down into the nano-regime from our previous work could potentially yield positive advancements in the field of planar chromatography.

b. Stacking

The decrease in phase ratio as one moves from the origin to the solvent front in planar chromatography is well documented for traditional systems [16, 17, 20, 22, 23]. The capillary action driven solvent flow replenishes evaporated solvent most effectively from the solvent reservoir side of the system. The relative effect of evaporation is likely exacerbated for our NTLC (1-2µm depth) relative to UTLC or conventional TLC due to the shallowness of the platform. If we consider Equations [5] and [6], as values for the phase ratio β increase smaller k' values for a given partition coefficient (Kc) are observed and this increases flow relative to the mobile phase velocity (v_{mp}) in the band involved (i.e.., the zone behind band center can move faster than the zone in front).

$$k' = K_C \frac{V_S}{V_M} \quad \text{or} \quad \frac{K_C}{\beta} \qquad [5]$$

$$V_{zone} = \frac{v_{mp}}{(1 + k')} \qquad [6]$$

SI Figure 4 shows stacking effects for one of our test analytes for both TLC and NTLC. The stacking helps to counteract the traditional Van Deemter band broadening contributions and for the NTLC case plate heights that are significantly lower in the direction of propagation than predicted from the Van Deemter Equation. A beneficial stacking effect is seen in the resolution of the bands in Figure 4 B for which isotopic band broadening would have left the bands largely unresolved.

c. Focusing

The focusing effects observed during the band drying are not easily understood for our complex morphologies. The traditional coffee ring effect moves solute (usually particles) toward the perimeter of a drying droplet. This occurs as the droplet edge is pinned and evaporation at the perimeter produces a replenishing outward flow from the center[23]. In some cases such flows can be reversed by Marangoni and other effects[24]. In fact we have observed preferred perimeter deposition of solute at times during sample spotting. SI Figure 5 is one of the more informative of these observations. For this spotting procedure we take advantage of the superhydrophobic nature of the array and continuously deliver sample solution from

a small gauge needle syringe into a very small (typically 200-250 μm) spot on the array[1]. The process can take tens of seconds during which fresh solution is added and replenishes evaporation at the perimeter of the spot. As evaporation occurs at the perimeter, solute should be driven by phase distribution into the stationary phase leaving the equivalent of a coffee ring effect. However, if the perimeter becomes saturated then the solute will be retained in the liquid phase and this can lead to a more uniform spot or even a preference of solute in the center of the spot. These effects seem to occur in SI Figure 5 for a two component mixture observed with microscope settings that observe both dyes. The red Rhodamine dye has a larger k', a lower concentration, and appears more at the perimeter. Conversely the FITC green dye has a smaller k' (less affinity for the stationary phase), a higher concentration to facilitate detection, and appears more in the center of the spot. These observations of phase distribution and non-linear isotherm behavior may help explain the focusing shown in Figure 3B, C and 4A. In Figure 3B a very high concentration of dye was used to observe the process in real time and it appears that the dye is being swept along with the receding drying front. Presumably the stationary phase is saturated to the right of the front in the figure. In Figure 3C the R_f is approximately 0.5 (apparent H ~ 100nm). whereas in Figure 4A the focused band is near the solvent front and is focused more tightly (apparent H < 100nm). Clearly the focusing effect is very system and condition dependent and it remains to be determined if it can be harnessed for practical chromatographic good.

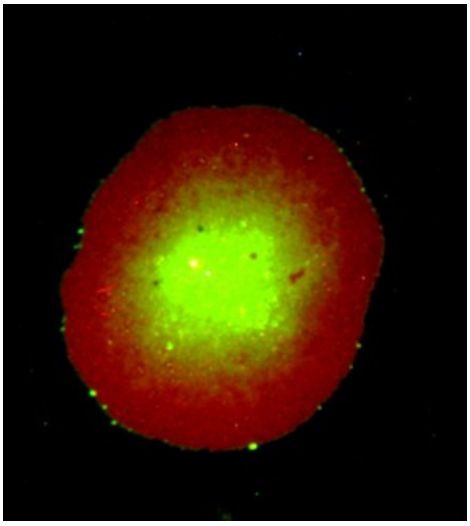

Figure 5: Image of spotted FITC and Rhodamine sample showing spatially defined drying.

1. C. E. Freye, N. A. Crane, T. B. Kirchner and M. J. Sepaniak, *Analytical Chemistry*, 2013, 85, 3991-3998.
2. N. V. Lavrik, L. C. Taylor and M. J. Sepaniak, *Lab on a Chip*, 2010, 10, 1086-1094.
3. N. V. Lavrik, L. T. Taylor and M. J. Sepaniak, *Analytica Chimica Acta*, 2011, 694, 6-20.
4. L. C. Taylor, T. B. Kirchner, N. V. Lavrik and M. J. Sepaniak, *Analyst*, 2012, 137, 1005-1012.
5. L. C. Taylor, N. V. Lavrik and M. J. Sepaniak, *Analytical Chemistry*, 2010, 82, 9549-9556.
6. W. De Malsche, D. Clicq, V. Verdoold, P. Gzil, G. Desmet and H. Gardeniers, *Lab on a Chip*, 2007, 7, 1705-1711.
7. W. De Malsche, S. De Bruyne, J. O. De Beeck, S. Eeltink, F. Detobel, H. Gardeniers and G. Desmet, *Journal of Separation Science*, 2012, 35, 2010-2017.
8. W. De Malsche, H. Eghbali, D. Clicq, J. Vangelooven, H. Gardeniers and G. Desmet, *Analytical Chemistry*, 2007, 79, 5915-5926.
9. W. De Malsche, H. Gardeniers and G. Desmet, *Analytical Chemistry*, 2008, 80, 5391-5400.
10. J. De Smet, P. Gzil, N. Vervoort, H. Verelst, G. V. Baron and G. Desmet, *Analytical Chemistry*, 2004, 76, 3716-3726.
11. S. M. Wells, S. D. Retterer, J. M. Oran and M. J. Sepaniak, *ACS Nano*, 2009, 3, 3845-3853.
12. R. L. Agapov, B. Srijanto, C. Fowler, D. Briggs, N. V. Lavrik and M. J. Sepaniak, *Nanotechnology*, 2013, 24, 505302-505311.
13. J. J. Charlton, N. Lavrik, J. A. Bradshaw and M. J. Sepaniak, *ACS Applied Materials & Interfaces*, 2014.
14. M. C. Hennion, C. Picard and M. Caude, *Journal of Chromatography*, 1978, 166, 21-35.
15. F. Gritti and G. Guiochon, *Journal of Chromatography A*, 2012, 1221, 2-40.
16. C. F. Poole, *Journal of Chromatography A*, 2003, DOI: 10.1016 /S0021-9673(03)00435-7, 963-984.
17. S. K. Poole and C. F. Poole, *Journal of Chromatography A*, 2011, 1218, 2648-2660.
18. G. Guiochon and S. Antoine, *Journal of Chromatographic Science*, 1978, 16, 470-481.
19. G. Deininger, *Chromatographia*, 1976, 9.
20. C. F. Poole, *The Essence of Chromatography*, Elsevier Science B.V., Amsterdam, 2003 edn., 2003.
21. T. T. Mai, C. Q. Lai, H. Zheng, K. Balasubramanian, K. C. Leong, P. S. Lee, C. Lee and W. K. Choi, *Langmuir*, 2012, 28, 11465-11471.
22. J. M. Miller, *Chromatography: Concepts and Contrasts*, John Wiley & Sons, Inc., Hoboken, NJ, 2005.
23. P. S. Variyar, S. Chatterjee and A. Sharma, in *High-Performance Thin-Layer Chromatography (HPTLC)*, ed. M. Srivastava, Springer, 2011, ch. 2.